Catalysis Science & Technology

ROYAL SOCIETY OF CHEMISTRY

COMMUNICATION

View Article Online
View Journal | View Issue

Cite this: *Catal. Sci. Technol.*, 2025, 15, 33

Received 22nd October 2024,
Accepted 18th November 2024

DOI: 10.1039/d4cy01272k

rsc.li/catalysis

Correlation of the catalytic performance with $Ru^{\delta+}$ species on Ru/Nb_2O_5 in furfural aqueous reductive conversion†

Yulong Deng,[abc] Binyu Zhang,[abc] Huiru Wu,[abc] Zhuo He,[abc] Xiaorui Du,[abc] Jiayi Ou,[abc] Tianyu Ren,[bc] Haiyong Wang,[abc] Yuhe Liao,[abc] Qiying Liu,*[d] Chenguang Wang *[abc] and Yanbin Cui *[abc]

Ru/Nb_2O_5 is effective for furfural aqueous reductive conversion. Systematic characterization, kinetic studies and *in situ* DRIFT tests demonstrated that the $Ru^{\delta+}$ species abundance is highly correlated with the adsorption behavior of the substrate, key intermediate and product (furfural, 2-cyclopentenone, and cyclopentanone), which governs the FFR conversion rate and cyclopentanoid product selectivity.

1. Introduction

Furfural (FFR) is one of the 12 most important biomass-derived platform compounds, which can be industrially prepared from hemicellulose in large quantities.[1] Reductive conversion of FFR has been extensively investigated to prepare diverse value-added chemicals, among which cyclopentanoid compounds (such as cyclopentanone (CPO) and cyclopentanol (CPOL)) are of significant interest due to their wide range of applications across various industrial sectors, such as fungicides, pharmaceuticals, rubber chemicals, and flavour and fragrance chemicals.[2,3] Since the first study reported by Hronec and co-workers on the aqueous phase conversion of FFR to CPO using carbon-supported precious metal catalysts,[4] numerous studies have been conducted to optimize catalyst design and streamline production processes.[5,6]

The reaction proceeds through a series of C=O hydrogenation, ring-opening, isomerization, dehydration and C=C hydrogenation steps. Therefore, to achieve high selectivity for cyclopentanoid products, it is essential to develop a catalyst that preferentially hydrogenates the C=O bond over the C=C bond and excels in acid-catalysed ring rearrangement. Ru as an oxophilic metal with excellent H_2 dissociation and deoxygenation activity is one of the most widely applied metal catalysts for aqueous reductive conversion of biomass-derived carbonyl compounds.[7–9] Support matrices such as metal oxides can act as promoters by anchoring metal species, introducing defects, interacting with supported metal and stabilizing particular oxidation states of the active metal.[10] Nb_2O_5 is widely applied as a stable support in catalytic processes involving the synergy of Brønsted and Lewis acid sites, making Ru/Nb_2O_5 a versatile catalyst with outstanding performance for hydrodeoxygenation (HDO) of a variety of substrates, such as phenols,[11] alkenes,[12] ethers,[13] and particularly unsaturated aldehydes.[14]

The electronic structure is a key factor determining the intrinsic activity of the catalyst because it affects the stability of the transition state during the reaction and determines the interaction strength between the catalyst and reactants. Numerous studies reported that electron-deficient $M^{\delta+}$ species on the catalyst surface is responsible for the high selectivity toward FAOL conversion of furfural.[15,16] The Nb_2O_5 support could boost the HDO performance of Ru by forming a $Ru–RuO_x–Nb_2O_5$ interface through tunable electron transfer between the support and metal,[17,18] which is critical in manipulating substrate adsorption behaviour. Moreover, the desorption behaviour of CPO can also be tuned on electron-deficient metal species derived from heteroatom doping, which further governs the distribution of over-hydrogenation products.[15] However, the impact of the electronic structure of various Ru species on cyclopentanoid compounds from FFR aqueous reductive conversion has been elusive, and the correlative analysis between the abundance of reactive $Ru^{\delta+}$ species and catalytic performance is scarcely investigated.

[a] *School of Energy Science and Engineering, University of Science and Technology of China, Hefei 230026, PR China*
[b] *CAS Key Laboratory of Renewable Energy, Guangzhou Institute of Energy Conversion, Chinese Academy of Sciences, Guangzhou 510640, PR China. E-mail: wangcg@ms.giec.ac.cn, cuiyb@ms.giec.ac.cn*
[c] *Guangdong Provincial Key Laboratory of Renewable Energy, Guangzhou 510640, P.R. China*
[d] *Jiangsu Co-Innovation Centre of Efficient Processing and Utilization of Forest Resources, International Innovation Centre for Forest Chemicals and Materials, Nanjing Forestry University, Nanjing 210037, PR China. E-mail: liuqy@njfu.edu.cn*
† Electronic supplementary information (ESI) available. See DOI: https://doi.org/10.1039/d4cy01272k

In this contribution, a series of Ru/Nb_2O_5 catalysts with varied reduction temperatures were employed as model catalysts to investigate the metal–support interaction in FFR reductive conversion. Systematic characterization was applied to investigate the physicochemical properties of the as-prepared catalysts, and the abundance of partially oxidized $Ru^{\delta+}$ species was analysed by XPS and H_2-TPR on activated catalysts. The kinetic study profiled the transition from the substrate to key intermediates, and to final products, providing a comprehensive perspective to investigate the relationship between the $Ru^{\delta+}$ species and catalytic performance. The role of $Ru^{\delta+}$ species in FFR conversion and product selectivity was further elucidated by interpreting the adsorptive behaviour of FFR, furfural alcohol (FAOL), 2-cyclopentenone (CPEO), and CPO using *in situ* DRIFTS.

2. Results and discussion

2.1 FFR aqueous reductive conversion using various Ru/MO_x catalysts

Different types of Ru/MO_x catalysts using various supports (MoO_3, TiO_2, Al_2O_3, ZrO_2, Nb_2O_5) with consistent Ru loading were prepared, to assess the impact of metal oxide supports on product distribution in FFR conversion (Table 1). The carbon balance of Ru supported on MoO_3, Al_2O_3 and ZrO_2 was lower than 75%, indicating that significant furfural loss takes place due to coking. Ru/MoO_3 and Ru/Al_2O_3 also resulted in the formation of a considerable amount of tetrahydrofurfuryl alcohol (THFAOL) with a respective yield of 31.6% and 10.0%, associated with excessive hydrodeoxygenation of the furan ring. Considerable accumulation of the FAOL intermediate (27.6%) was detected for Ru/ZrO_2, which is associated with limited acidic strength that is less effective in promoting the Piancatelli rearrangement for further conversion.[19,20] In comparison, Ru/Nb_2O_5 showed a full conversion of FFR and a much higher carbon balance (90.2%), and the overall yield of and selectivity to cyclopentanoid products reached up to 87.4% and 96.9%, respectively.

Due to its satisfactory catalytic performance, Ru/Nb_2O_5 was selected as the model catalyst for further investigation *via* material manipulation techniques. The reaction temperature and pressure were optimized for Ru/Nb_2O_5 catalysed FFR conversion (Fig. S1†). At low reaction temperatures, considerable FAOL accumulation was observed due to the low efficiency in initiating the acid-driven ring rearrangement.[21] However, carbon balance dropped sharply at elevated reaction temperatures, associated with extensive self-polymerization of FFR and formation of humins under such conditions.[22,23] Low initial hydrogen pressure was shown to be ineffective in hydrogenating the key intermediates, leaving considerable amounts of FAOL and CPEO unconverted, while over hydrogenation of the furan ring occurred and generated the THFAOL by-product when the hydrogen pressure was beyond 5 MPa. Overall, 4 MPa and 160 °C were selected due to the satisfactory conversion, carbon balance and cyclopentanoid product selectivity.

2.2 Structural and textural characterization of Ru/Nb_2O_5 catalysts

A series of Ru/Nb_2O_5 catalysts were prepared by tuning the reduction temperatures following an identical calcination protocol. As shown in Fig. S2,† the SEM images of all Ru/Nb_2O_5 catalysts present similar morphological features, and the TEM images show that the Ru nanoparticle size is around 5 nm, with the *d*-spacing of 0.201 nm of the Ru nanoparticles in the catalysts corresponding to the Ru(101) plane. The amount and dispersion of Ru were measured by ICP-OES and H_2 pulse chemisorption (Table S1†). The actual Ru loading of all Ru/Nb_2O_5 catalysts matches well with their nominal Ru loading, indicating negligible Ru leaching or Nb_2O_5 loss during the material synthesis process. No significant difference in metal dispersion was found among Ru/Nb_2O_5 catalysts with different reduction temperature treatments, indicating the excellent stabilization capability of Nb_2O_5 as a metal support.

No characteristic XRD patterns of Ru or RuO_2 phases are detected for all catalysts, indicating that Ru particles are highly dispersed on the support with their sizes below the limit of phase detection (Fig. 1a). The sharp peaks for all samples indicate the high degree of crystallinity of the Nb_2O_5 support. Catalysts reduced at temperatures below 650 °C share multiple sharp diffraction peaks of different planes of Nb_2O_5 (PDF#72-1484) and $Nb_{16.8}O_{42}$ (PDF#71-0336). In Ru/Nb_2O_5-H(850), the XRD pattern exhibits new diffraction peaks at 26.0°, 35.2°, and 52.1°, corresponding to the presence of a

Table 1 The hydrodeoxygenation of furfural over various catalysts

Entry	Catalyst	Conversion of FFR (%)	Yield (C-mol%)				Carbon balance of the product (C-mol%)
			THFAOL	FAOL	CPO	CPOL	
1	5% Ru/MoO_3	>99.9	10.0	—	0.2	60.5	70.7
2	5% Ru/Al_2O_3	>99.9	31.6	—	0.8	42.5	74.9
3	5% Ru/ZrO_2	>99.9	—	27.6	0.2	43.4	71.2
4	5% Ru/TiO_2	25.9	—	2.0	23.7	—	25.7
5	5% Ru/Nb_2O_5	>99.9	—	2.8	21.1	66.3	90.2
6	Pristine Nb_2O_5	1.9	—	—	—	—	—
7	Nb_2O_5-H(450)	3.1	—	—	—	—	—

Catalyst preparation conditions: calcined at 500 °C and reduced at 450 °C. Reaction conditions: 0.20 g furfural, 0.04 g catalyst, 20 mL of H_2O, *p* (initial, H_2) = 4.0 MPa, reaction temperature is 160 °C, heating rate = 5 °C min^{-1}, stirring speed = 800 rpm, reaction time = 6 h.

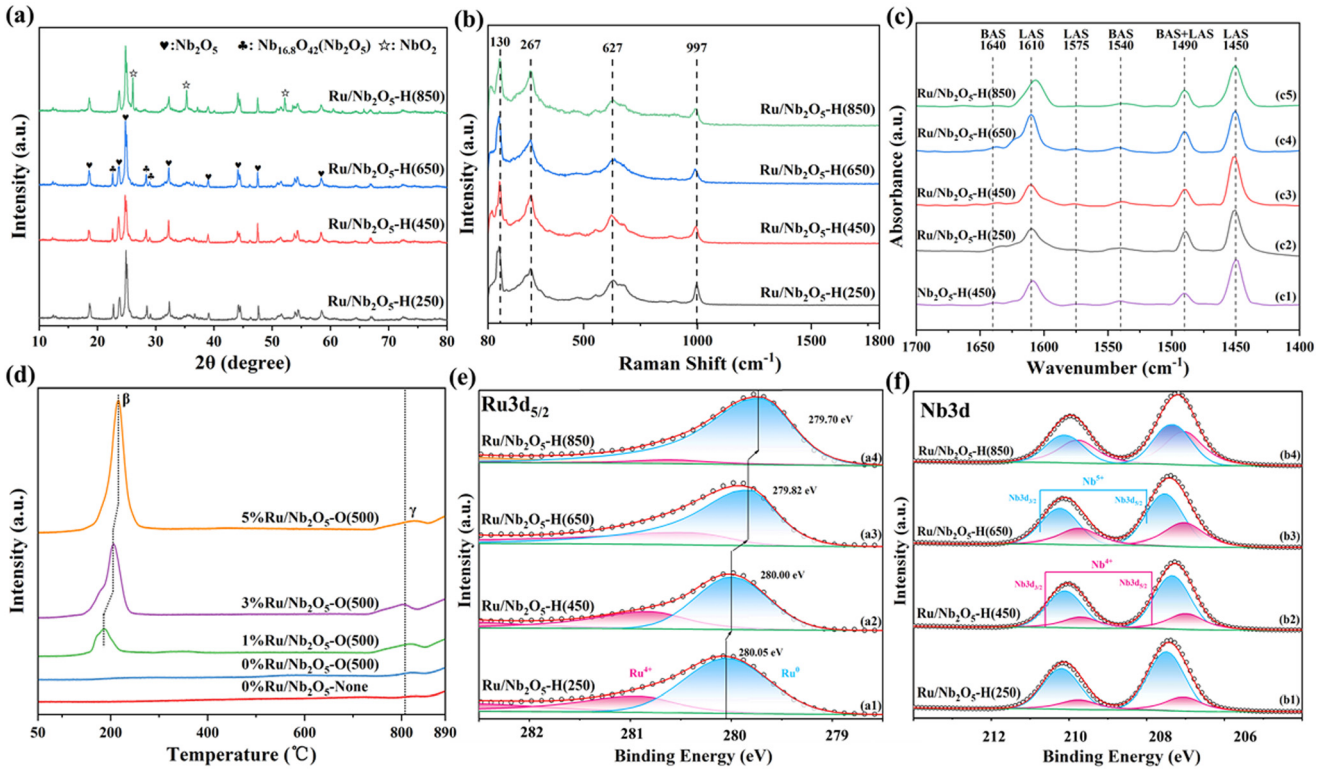

Fig. 1 Material characterization of various 1% Ru/Nb_2O_5 catalysts reduced at varied temperatures. (a) XRD patterns, (b) Raman spectra, (c) Py-IR spectra at a desorption temperature of 150 °C, (d) H_2-TPR profile, XPS results and peak fitting curves of (e) Ru3d and (f) Nb3d.

newly formed NbO_2 phase (PDF#71-0020). The BET test indicates that the crystallized support showed a very limited porous structure (Table S2†). In Fig. 1b, the Raman spectra show a prominent vibrational peak centred at 130 cm^{-1}, attributed to the stretching vibration between the Nb–Nb bond.[24,25] The Raman vibrational peak at 267 cm^{-1} and 627 cm^{-1} is assigned to the bending vibration and bridging vibration mode of the Nb–O–Nb bond, respectively.[26,27] The vibrational peak at ~997 cm^{-1} is attributed to the symmetric stretching vibration mode of the Nb=O bond between edge-sharing NbO_6 octahedra, which contribute to Lewis acidic sites (LASs) on the surface.[28,29] Fig. 1c displays the Py-FTIR spectra of Ru/Nb_2O_5 catalysts after desorption at 150 °C, showing characteristic bands for Lewis acidic sites (1450 cm^{-1}, 1610 cm^{-1}) and minor bands (1490 cm^{-1}) for both Brønsted and Lewis acidic sites.[30] For all tested Ru/Nb_2O_5 catalysts, LASs present the dominant acid species and their density remains essentially consistent. The LA abundant sites in Nb_2O_5 promote cyclopentanoid selectivity by suppressing hydrogenation to THFAOL, as reported in previous research.[31] H_2-TPR shows a dominant H_2 uptake peak (β peak) at 193 °C, and the reduction peak slightly shifts to a higher temperature as the metal loading increases, which is associated with the broader size distribution. The γ reduction peak centred at 814 °C is attributed to the removal of surface oxygen (Fig. 1d).[32,33]

The surface electronic structure/chemical states of Ru and Nb were determined by X-ray photoelectron spectroscopy (XPS). In Fig. 1e, the deconvoluted peaks at ~280.0 eV and ~280.8 eV are assigned to the Ru^0 $3d_{5/2}$ state and $Ru^{\delta+}$ $3d_{5/2}$ state, respectively.[34] With the increase of reduction temperature, the proportion of Ru^0 in total ruthenium species increases along with a shift to a lower binding energy, which is associated with intensified electron transfer from the support to metallic Ru sites.[35,36] Detailed Nb 3d spectra of these Ru/Nb_2O_5 catalysts present a broad Nb $3d_{5/2}$ peak between 205 and 209 eV (Fig. 1f), which can be deconvoluted to two peaks at ~207.1 and ~207.4 eV, respectively, corresponding to Nb^{4+} and Nb^{5+} states.[37] The ratio of the Nb^{4+} peak increases gradually with reduction temperature. As a result of the intensified electron transfer effect, the $Ru^{\delta+}/(Ru^0 + Ru^{\delta+})$ ratio decreased from 0.41 to 0.08, with the reduction temperature increasing from 250 °C to 850 °C (Table S3†).

2.3 Kinetic study of FFR reductive conversion over tailored Ru/Nb_2O_5 catalysts

The batch study showed that the FFR conversion drops as the catalyst reduction temperature increases, while the CPO selectivity ascends from 23% for 1% Ru/Nb_2O_5-H(250) to 98% for 1% Ru/Nb_2O_5-H(850) (Fig. S3†). In contrast, the CPO selectivity decreases as the metal loading increases to 3% with a full conversion of FFR obtained, indicating that reactive Ru species can be simultaneously tuned by reduction temperature and Ru loading. Such notable results promote

us to further investigate the changes of FFR conversion and product selectivity with the reaction time (Fig. 2). Among the tested catalysts, 1% Ru/Nb_2O_5-H(250) showed an efficient conversion toward FAOL, CPEO and CPO in a sequential order, and high FFR conversion (99%) and high CPO selectivity (93%) were achieved at 300 min. After that, the selectivity to CPO dropped sharply as the reaction proceeded, due to the concurrent formation of CPOL. For the 1% Ru/Nb_2O_5-H(450) catalyst, it took a longer reaction time for CPO generation, achieving a high selectivity of 90% toward CPO after 10 h, with a very low level of CPOL found. The other two catalysts reduced at higher temperatures (650 °C and 850 °C) displayed a slower rate for FFR conversion and CPO formation, with negligible CPOL detected over the whole reaction span (Fig. 2), indicating that over hydrogenation of the C=O bond of CPO was suppressed due to the retarded conversion of the substrate and intermediates.

The apparent reaction rate constants for FFR conversion of various Ru/Nb_2O_5 catalysts were calculated using the pseudo-first-order model (Table S4†), assuming that hydrogen is in significant excess.[36,37] The calculated reaction rate constant decreases as the reduction temperature of Ru/Nb_2O_5 catalysts increases (Fig. 3a). Considering the similar properties of the Ru/Nb_2O_5 catalysts, such as porosity, surface acidity, geometric features and dispersion, we infer that the main factor attributed to the different catalytic performances is the electronic structures of reactive Ru species. XPS results showed that electron transfer from the Nb_2O_5 carrier to the Ru metal active site was promoted, leading to a decreased ratio of $Ru^{\delta+}$ among Ru species. It has been extensively reported that electron-deficient metal sites are critical for furfural adsorption, and partially oxidized $Ru^{\delta+}$ sites were also reported as reactive sites dominating furfural conversion.[15,38]

To quantitatively interpret the role between active sites and catalytic activity, the activated catalysts were subjected to H_2-TPR analysis, and hydrogen uptake was used to determine the abundance of reactive $Ru^{\delta+}$ species in Ru/Nb_2O_5 catalysts (Fig. 3b, Table S5†). No β reduction peak was found in the activated Ru/Nb_2O_5 catalysts, indicating that the dominant species in these reduced catalysts is metallic Ru. By contrast, a distinct α reduction peak can be observed at around 100 °C for all reduced Ru/Nb_2O_5 catalysts, which is attributed to the reduction of the reactive $Ru^{\delta+}$ species on the surface that can be easily oxidized upon air exposure.[39] The hydrogen consumption of the α reduction peak decreased gradually with the increase of reduction temperature, indicating that the abundance of $Ru^{\delta+}$ species on the catalyst surface was negatively affected by reduction temperature.

This is consistent with the observed trend presented by XPS analysis. Notably, a good correlation between reactive $Ru^{\delta+}$ species on the surface of the Ru/Nb_2O_5 series catalysts and the apparent reaction rate constant k for FFR conversion was found, with the corresponding fitting curve's correlation coefficient R^2 = 0.975 (Fig. 3c). The H_2-TPR hydrogen consumption increases as the reduction temperature of the catalyst decreases, and the conversion rate of FFR by the catalyst increases accordingly.

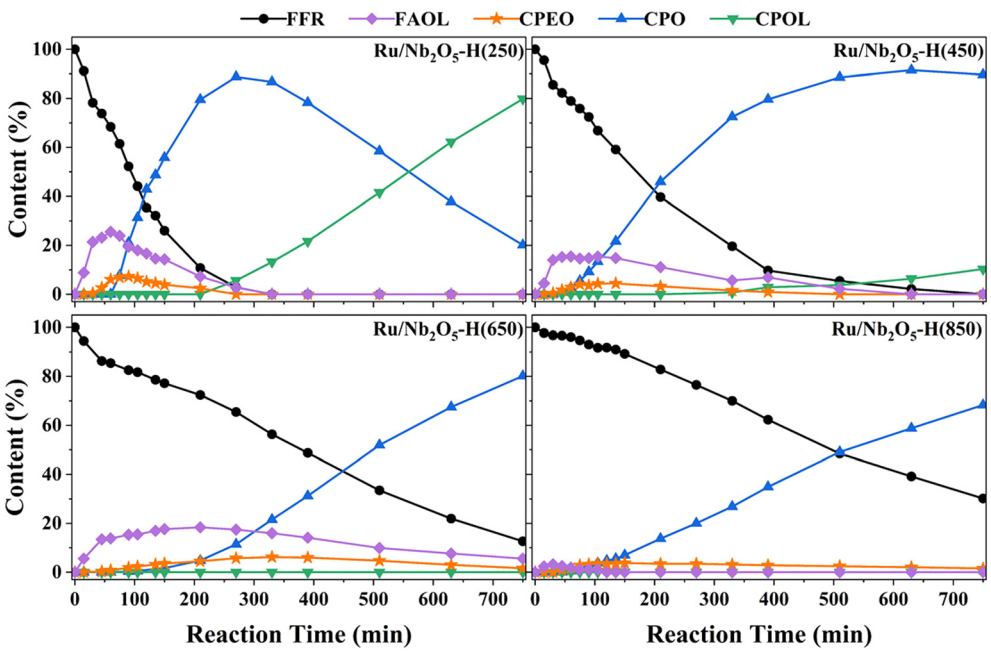

Fig. 2 Catalytic kinetics of FFR aqueous reductive conversion over various Ru/Nb_2O_5 catalysts. Reaction conditions: 2.00 g furfural, 0.40 g catalyst, 200 mL of H_2O, p (initial, H_2) = 5.0 MPa, the initial reaction temperature is 25 °C, T = 160 °C, heating rate = 4.5 °C min^{-1}, stirring speed = 800 rpm, reaction time = 720 min.

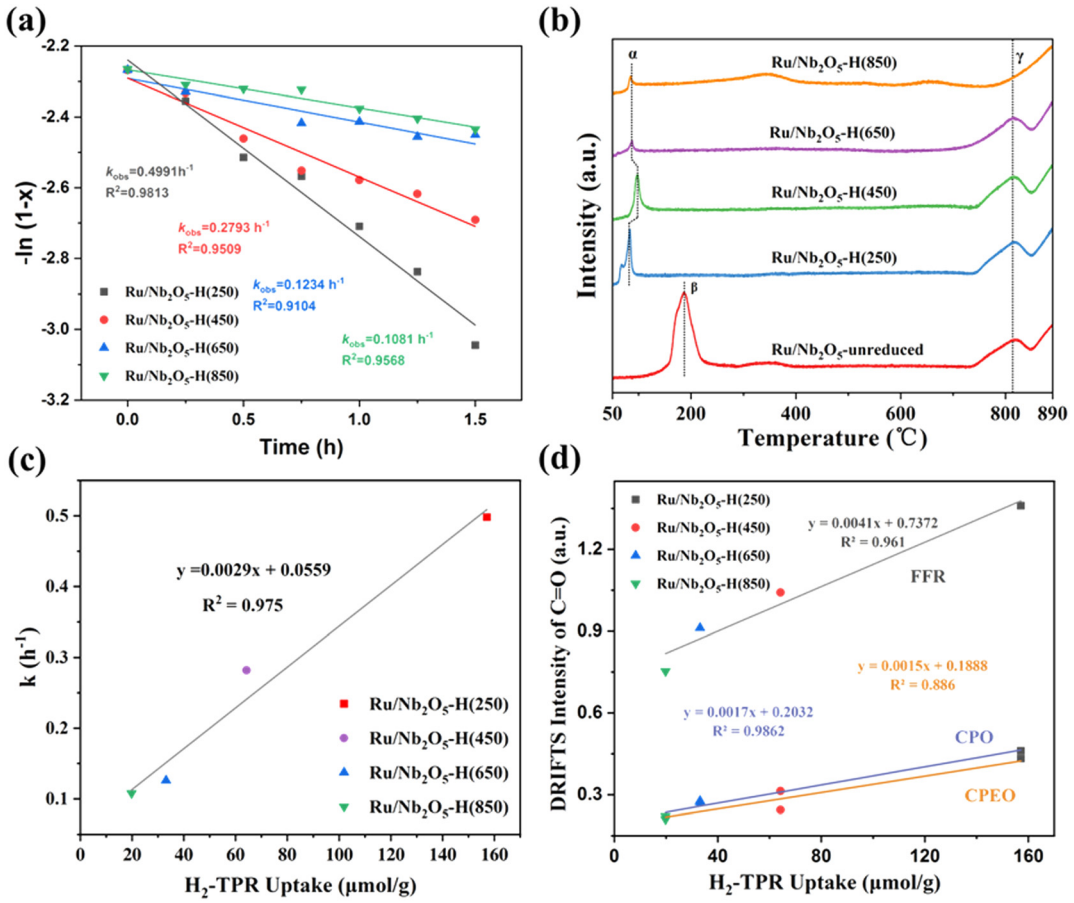

Fig. 3 (a) Kinetic fitting curves of kinetic data of the Ru/Nb_2O_5 catalyst, *x* stands for FFR conversion; (b) H_2-TPR profiles for 1% Ru/Nb_2O_5 catalysts with varied reduction temperatures; (c) the fitting curves of H_2-TPR uptake of the α peak and FFR reaction rate constant; (d) the fitting curves of H_2-TPR uptake and the intensity of C=O adsorption of furfural.

2.4 Adsorptive behaviour of the substrate, intermediates, and product over Ru/Nb_2O_5

Time-resolved *in situ* DRIFTS was used to study the adsorption behaviours of the substrate, key intermediates and product on different Ru/Nb_2O_5 catalysts (Fig. 4). For FFR, there were two possible adsorption patterns of the carbonyl group on Ru nanoparticles: direct adsorption by carbonyl oxygen atoms *via* η^1(O) or bi-coordination adsorption through both carbon and oxygen atoms *via* η^2(C–O).[40] The wavenumber of the C=O infrared vibration was found at 1710 cm^{-1} using a control adsorbent, indicating that FFR molecules solely undergo physical adsorption on these surfaces (Fig. S4†).[41] Fig. 4 presents a signal peak at 1716 cm^{-1} that is assigned to the C=O stretching vibration of gas-phase furfural at the early stage of the adsorption process. As the adsorption proceeds, the wavenumber assigned to C=O vibration is notably redshifted to around 1673 cm^{-1} due to weakened adsorbed C–O stretching,[42] whereas the position of the C=C stretching in the furan ring (1400 cm^{-1}) group is invariant (Fig. S5†). This suggests that the FFR is perpendicularly adsorbed and forms an η^1(O) surface intermediate.[43,44]

Notably, the retention time of the C=O signal upon heating treatment decreases from 13 min (Ru/Nb_2O_5-H(250)) to 3.5 min (Ru/Nb_2O_5-H(850)), indicating weaker FFR adsorption with increasing reduction temperature due to decreasing active $Ru^{\delta+}$ sites. Also, the intensity of the characteristic C=O signal after consistent heating treatment displayed a decreasing trend as the catalyst reduction temperature increases (Table S6†). In fact, a good linear fitting relationship was found between the H_2-TPR uptake and the adsorption intensity of the C=O group of FFR on the catalyst surface (Fig. 3d). These results indicate that the presence of active $Ru^{\delta+}$ sites is highly related to the substrate adsorption orientation and adsorption strength. Kim *et al.* reported that the oxygen atoms of the C=O groups of these carbonyl containing compounds preferentially adsorbed at the coordinatively unsaturated $Ru^{\delta+}$ sites in an η^1(O)-aldehyde configuration,[40] which is consistent with the result presented in our study. In comparison, the adsorption behaviour of FAOL onto different Ru/Nb_2O_5 catalysts showed no obvious difference. A strong signal assigned to –OH group adsorption centred at ~1000 cm^{-1} was detected, corresponding to the adsorption configuration of η^1(O)-alcohol hydroxyl of FAOL (Fig. S6†).[16] It has been reported

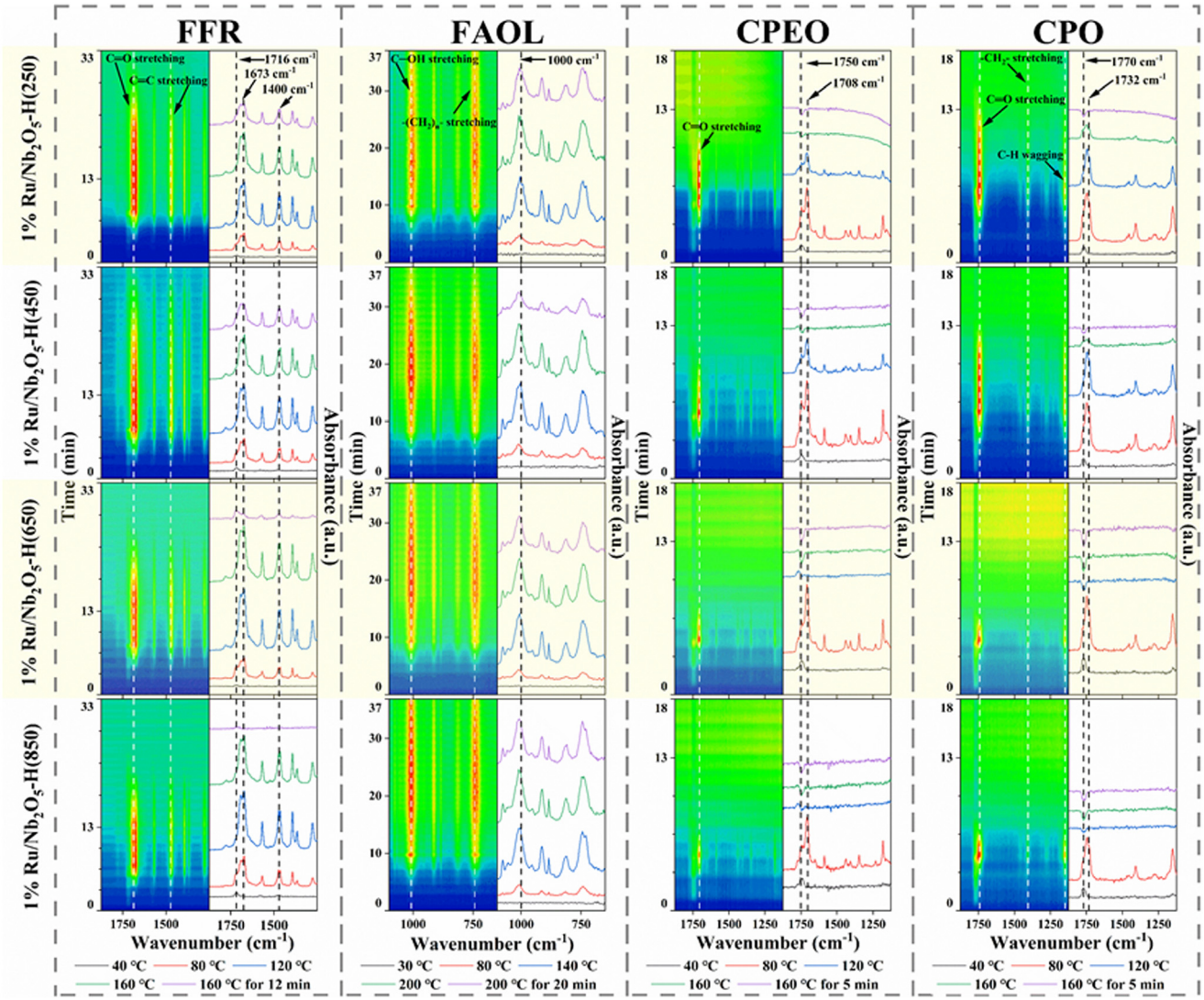

Fig. 4 Time-resolved *in situ* DRIFT spectra for FFR, FAOL, CPEO, and CPO adsorption over various 1% Ru/Nb_2O_5 catalysts reduced at varied temperatures. Note: FAOL was subjected to programmed heating to 200 °C, for detailed conditions see Fig. S5–S8.†

that the main sites for the adsorption of η^1(O)-alcohol hydroxyl groups in FAOL are Lewis acid sites.[24,45] This result is consistent with the Py-FTIR result that showed similar abundance and distribution of LA sites among the catalysts.

Similar adsorption tests were conducted for other carbonyl containing compounds CPEO and CPO (Fig. S7 and S8†). Both molecules show a band at around 1750 cm^{-1} attributed to ν(C═O),[46] and the peak shows a red-shift (30 cm^{-1}) with significant improvement of relative intensity, indicating chemically adsorbed carbonyl groups onto $Ru^{\delta+}$ sites. As the catalyst reduction temperature increases, the C═O signal intensity follows the same decreasing trend as that of FFR, correlating with the H_2-TPR uptake well (Fig. 3d). The decreasing CPO adsorption strength reveals that high CPO selectivity can be obtained by avoiding over-hydrogenation using a catalyst produced at elevated reduction temperature. The adsorptive behaviour of these different types of carbonyl containing intermediates and the target product affords a panoramic vision regarding FFR conversion and final product selectivity in aqueous reductive conversion processes.

3. Conclusions

In this contribution, we investigated selective production of cyclopentanoid products from FFR using Ru/Nb_2O_5 model catalysts, with the interaction between the Ru site and the Nb_2O_5 support regulated through reduction temperature variation. The FFR conversion rate constant decreased as the reduction temperature increased, accompanied with increased CPO selectivity. Through various catalyst characterization techniques, it was confirmed that surface $Ru^{\delta+}$ species were inversely related to reduction temperature due to intensified electron transfer from the support to metal. The adsorption mode and strength of FFR, FAOL, CPEO, and CPO onto the surface of Ru/Nb_2O_5 catalysts were detected with *in situ* DRIFTS, revealing that carbonyl containing compounds (FFR,

CPEO, CPO) preferentially interact with $Ru^{\delta+}$ sites through an $\eta^1(O)$ configuration, and a positive correlation between adsorption intensity and $Ru^{\delta+}$ abundance was noted. We propose that in these Ru/Nb_2O_5 catalysts, the $Ru^{\delta+}$ sites coordinatively bind and activate the C=O group in the substrate, and the conversion rate of FFR and over-hydrogenation of CPO can be tuned through reduction temperature-dependent Ru^0 and $Ru^{\delta+}$ distribution, thereby manipulating substrate conversion and product selectivity.

Data availability

The data that support the findings of this study are included within the article.

Conflicts of interest

There are no conflicts to declare.

Acknowledgements

This work was financially supported by the International Science and Technology Innovation Cooperation Program of the National Key Research and Development Plan of China (2021YFE0114400) and the Guangdong Basic and Applied Basic Research Foundation of China (2023A1515110745). The authors would also like to thank the Analysis and Test Centre at Guangzhou Institute of Energy Conversion for their support in spectrometry analysis.

References

1 X. Li, P. Jia and T. Wang, *ACS Catal.*, 2016, **6**, 7621–7640.
2 S. Kotha and Y. Tangella, *Synlett*, 2020, **31**, 1976–2012.
3 V. B. Kurteva and C. A. M. Afonso, *Chem. Rev.*, 2009, **109**, 6809–6857.
4 M. Hronec and K. Fulajtarova, *Catal. Commun.*, 2012, **24**, 100–104.
5 G.-S. Zhang, M.-M. Zhu, Q. Zhang, Y.-M. Liu, H.-Y. He and Y. Cao, *Green Chem.*, 2016, **18**, 2155–2164.
6 P. Pan, W.-Y. Xu, T.-J. Pu, X.-D. Wang, X.-J. Pei, F. Tang and Y.-S. Feng, *ChemistrySelect*, 2019, **4**, 5845–5852.
7 R. Fang, H. Liu, R. Luque and Y. Li, *Green Chem.*, 2015, **17**, 4183–4188.
8 P. Panagiotopoulou, N. Martin and D. G. Vlachos, *ChemSusChem*, 2015, **8**, 2046–2054.
9 F. Liu, Q. Y. Liu, J. M. Xu, L. Li, Y. T. Cui, R. Lang, L. Li, Y. Su, S. Miao, H. Sun, B. T. Qiao, A. Q. Wang, F. Jérôme and T. Zhang, *Green Chem.*, 2018, **20**, 1770–1776.
10 Z. Gao, L. Yang, G. L. Fan and F. Li, *ChemCatChem*, 2016, **8**, 3769–3779.
11 R. Huang, O. Kwon, C. Lin and R. J. Gorte, *J. Catal.*, 2021, **398**, 102–108.
12 T. Uchijima, *Catal. Today*, 1996, **28**, 105–117.
13 H. Ali, T. Vandevyvere, J. Lauwaert, S. K. Kansal, M. K. K. Sabbe, S. Saravanamurugan and J. W. W. Thybaut, *Catal. Sci. Technol.*, 2023, **13**, 1140–1153.
14 J. Fontana, C. Vignado, E. Jordao, F. C. A. Figueiredo and W. A. Carvalho, *Catal. Today*, 2011, **172**, 27–33.
15 W. C. Wang, H. K. Zhang, Y. D. Wang, F. Y. Zhou, Z. Y. Xiang, W. B. Zhu and H. L. Wang, *J. Energy Chem.*, 2024, **92**, 43–51.
16 N. Karanwal, R. G. Kurniawan, S. K. Kwak and J. Kim, *Chem. Eng. J.*, 2024, **498**, 155603.
17 Y. Xin, L. Dong, Y. Guo, X. Liu, Y. Hu and Y. Wang, *J. Catal.*, 2019, **375**, 202–212.
18 R. Tu, W. Lv, Y. Sun, Y. J. Wu, Y. W. Wu, X. D. Fan, E. C. Jiang, Q. Lu and X. W. Xu, *Chem. Eng. J.*, 2023, **453**, 139718.
19 Y. Yang, Z. Du, Y. Huang, F. Lu, F. Wang, J. Gao and J. Xu, *Green Chem.*, 2013, **15**, 1932–1940.
20 C. A. M. R. van Slagmaat, J. Noordijk, L. G. Monsegue, S. Mogensen, D. Hadavi, P. Han, P. J. L. M. Quaedflieg, G. K. M. Verzijl, P. L. Alsters and S. M. A. De Wildeman, *Green Chem.*, 2021, **23**, 7100–7114.
21 V. Ranaware, R. G. Kurniawan, D. Verma, S. K. Kwak, B. C. Ryu, J. W. Kang and J. Kim, *Appl. Catal., B*, 2022, **318**, 121838.
22 S. Karnjanakom, A. Bayu, P. Maneechakr, C. Samart, S. Kongparakul and G. Guan, *ACS Sustainable Chem. Eng.*, 2021, **9**, 14170–14179.
23 X. Hu, C. Lievens, A. Larcher and C.-Z. Li, *Bioresour. Technol.*, 2011, **102**, 10104–10113.
24 U. Balachandran and N. G. Eror, *J. Mater. Sci. Lett.*, 1982, **1**, 374–376.
25 T. Ikeya and M. Senna, *J. Non-Cryst. Solids*, 1988, **105**, 243–250.
26 F. D. Hardcastle and I. E. Wachs, *Solid State Ionics*, 1991, **45**, 201–213.
27 M. Ristic, S. Popovic and S. Music, *Mater. Lett.*, 2004, **58**, 2658–2663.
28 Y. Wang, S. Aghamohammadi, D. Li, K. Li and R. Farrauto, *Appl. Catal., B*, 2019, **244**, 438–447.
29 F. B. Passos, D. A. G. Aranda, R. R. Soares and M. Schmal, *Catal. Today*, 1998, **43**, 3–9.
30 M. H. Brijaldo, H. A. Rojas, Y. Xing, F. B. Passos and J. J. Martínez, *Catalysts*, 2024, **14**, 493.
31 Z. J. Yu, H. L. Tian, K. Sun, Y. W. Shao, L. J. Zhang, S. Zhang, P. G. Duan, Q. Liu, S. L. Niu, D. H. Dong and X. Hu, *Mol. Catal.*, 2020, **496**, 111187.
32 F. B. Noronha, D. A. G. Aranda, A. P. Ordine and M. Schmal, *Catal. Today*, 2000, **57**, 275–282.
33 K. A. Resende, F. B. Noronha and C. E. Hori, *Renewable Energy*, 2020, **149**, 198–207.
34 W. J. Guo, T. Tong, X. H. Liu, Y. Guo and Y. Q. Wang, *ChemCatChem*, 2019, **11**, 4130–4138.
35 J. Y. Shen, A. Adnot and S. Kaliaguine, *Appl. Surf. Sci.*, 1991, **51**, 47–60.
36 D. J. Morgan, *Surf. Interface Anal.*, 2015, **47**, 1072–1079.
37 T. A. Sasaki and Y. Baba, *Phys. Rev. B: Condens. Matter Mater. Phys.*, 1985, **31**, 791–797.
38 Z. Zhu and G. Xu, *Nanomaterials*, 2024, **14**(9), 788.

39 Y. Ma, B. Liu, M. Jing, R. Zhang, J. Chen, Y. Zhang and J. Li, *Chem. Eng. J.*, 2016, **287**, 155–161.
40 R. Insyani, A. F. Barus, R. Gunawan, J. Park, G. T. Jaya, H. S. Cahyadi, M. G. Sibi, S. K. Kwak, D. Verma and J. Kim, *Appl. Catal., B*, 2021, **291**, 120120.
41 S. Li, Y. Fan, C. Wu, C. Zhuang, Y. Wang, X. Li, J. Zhao and Z. Zheng, *ACS Appl. Mater. Interfaces*, 2021, **13**, 8507–8517.
42 H. Daly, H. G. Manyar, R. Morgan, J. M. Thompson, J. J. Delgado, R. Burch and C. Hardacre, *ACS Catal.*, 2014, **4**, 2470–2478.
43 Y. An, Q. Wu, L. Niu, C. Zhang, Q. Liu, G. Bian and G. Bai, *J. Catal.*, 2024, **429**, 115271.
44 J. Yu, Y. Yang, L. Chen, Z. Li, W. Liu, E. Xu, Y. Zhang, S. Hong, X. Zhang and M. Wei, *Appl. Catal., B*, 2020, **277**, 119273.
45 C. Verrier, S. Moebs-Sanchez, Y. Queneau and F. Popowycz, *Org. Biomol. Chem.*, 2018, **16**, 676–687.
46 E. Lemmon, M. McLinden, D. Friend, P. Linstrom and W. Mallard, *Thermophysical Properties of Fluid Systems*, Isobaric Properties for Water, 2011.

